ELSEVIER

Journal of Fluorine Chemistry 107 (2001) 205–214

JOURNAL OF FLUORINE CHEMISTRY

www.elsevier.com/locate/jfluchem

Structural influences of fluorine ligand in niobium cluster chemistry: crystal structures of $KNb_6Cl_{10}F_5$ and $CsNb_6Cl_8F_7$

S. Cordier*, O. Hernandez, C. Perrin

Laboratoire de Chimie du Solide et Inorganique Moléculaire, UMR CNRS 6511, Université de Rennes 1, Campus de Beaulieu, Avenue du Général Leclerc, 35042 Rennes Cedex, France

Accepted 18 June 2000

Abstract

We have synthesized by solid state chemistry and structurally characterized by single crystal X-ray diffraction two new cluster compounds, $KNb_6Cl_{10}F_5$ and $CsNb_6Cl_8F_7$. $KNb_6Cl_{10}F_5$ is a Ta_6Cl_{15} derived structure, whereas $CsNb_6Cl_8F_7$ exhibits a primitive framework derived from Nb_6F_{15}. In both structures, fluorine and chlorine are randomly distributed on the ligand positions, but in $CsNb_6Cl_8F_7$ fluorine fully occupies the apical positions. The comparison between the geometrical parameters of the title compounds and those observed in previously isolated Nb_6 chlorofluorides, halides and fluorides, allows specification of the influence of fluorine in niobium cluster chemistry.

Keywords: Cluster compounds; Fluorine effects; Niobium; Solid state structure; X-ray diffraction

1. Introduction

Complex fluorides $A_xM_yF_z$ (A = alkaline element; M = transition element) crystallize in numerous structure-types [1] which can be described as various stackings of $(MF_6)^{n-}$ octahedra sharing apices, edges or faces with adjacent groups. Additional A cations fill the vacancies of these architectures allowing the cohesion as well as the neutrality of the compounds. The type of condensation of these octahedra depends on the size of the M transition element. For instance, in Na_2NbF_7 [2] and $CoNbF_6$ [3], the NbF_6 octahedra preferentially share their apices. In complex fluorides, the high value of the redox potential of fluorine leads to a high oxidation state for the M cation, typically 4^+ or 5^+ for Nb and Ta.

In contrast to fluoroniobates and fluorotantalates, in many halides (halogen = Cl, Br, I) niobium and tantalum are well-known to remain in a low oxidation state forming metallic clusters characterized by M–M bonds. Edge-bridged octahedral cluster units of general formula $[(M_6L^i_{12})L^a_6]^{n-}$ (M = Nb, Ta; L^i = two-bonded inner halogen ligand; L^a = two-electron donor apical ligand (H_2O, OH^-, Cl^-, Br^- etc.)) (Fig. 1a) were characterized for the first time in solution [4]. They were subsequently encountered in solid state compounds in which the $[(M_6L^i_{12})L^a_6]^{n-}$ units can be isolated as found in $K_4Nb_6Cl_{18}$ [5], or connected by sharing some ligands with other adjacent units like for instance in Ta_6Cl_{15} [6], a chloride with the $Ta_6Cl^i_{12}Cl^{a-a}_{6/2}$ developed formula. The various types of possible connections are represented in Fig. 1b, according to the Schäfer notation [7]. Notice that the sharing of apical ligands (L^{a-a} ligands) between adjacent units in Nb_6 cluster chemistry is comparable to the sharing of fluorine apices of the NbF_6 octahedra in fluoroniobate chemistry.

This last decade, we have investigated niobium or tantalum cluster materials with the general formula $A_xREM_6X_{18}$ (A = monovalent cation; RE = rare earth cation; M = Nb, Ta; X = Cl, Br; $x = 0, 1, 2$) [8], $A_2REM_6X_{18-y}O_y$ ($y = 1, 3$) [9,10] and $REM_6X_{13}O_3$ [11] containing $(M_6L^i_{12})L^a_6$ units. Changing the nature of the different constituting elements has led to a set of isostructural compounds, allowing to perform a rigorous structural analysis of the unit deformation versus the VEC (valence electron concentration) per M_6 cluster, as well as versus the electronic and size effects of the ligands [8]. Let us recall that the VEC corresponds to the number of valence electrons available for the Nb–Nb bonds in the Nb_6 cluster. These electrons are located in the higher four bonding levels (a_{1g}, t_{2g}, t_{1u}, a_{2u} symmetry) of the $(Nb_6L_{18})^{n-}$ molecular orbital diagram. They have strong Nb–Nb bonding character and a Nb–L^i antibonding one [12]. Magnetic properties depend on the number of electrons

* Corresponding author.

0022-1139/01/$ – see front matter
PII: S0022-1139(00)00360-2

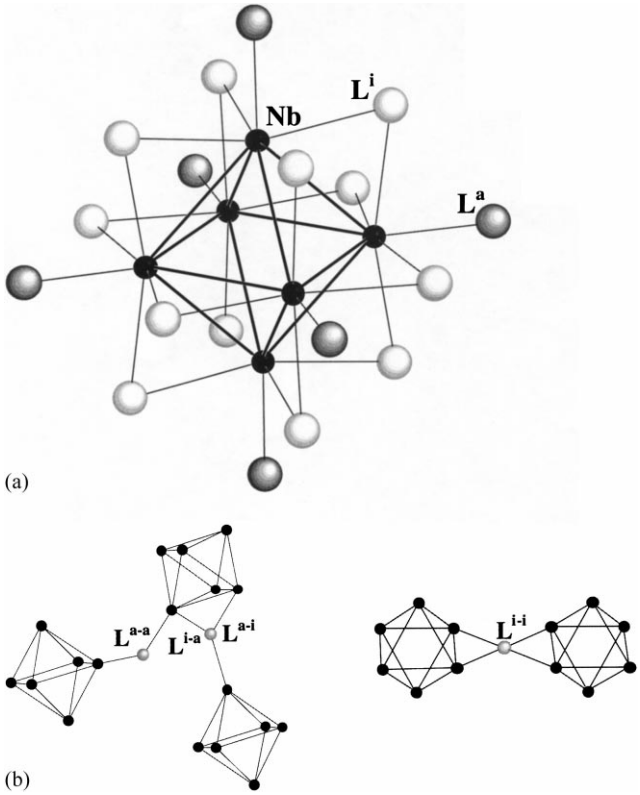

Fig. 1. (a) $(M_6L^i_{12})L^a_6$ unit; (b) schematic representation of the possible interconnections between units illustrating the Schäfer notation.

in the a_{2u} HOMO level. This level is filled and empty for 16 and 14 electrons per Nb_6 cluster, respectively, hence the unit is diamagnetic. For 15 electrons per Nb_6 cluster, one unpaired electron remains in this level, and the unit becomes magnetic (e.g. REM_6X_{18} ternary halides), but the steric hindrance of halogen ligands prevents cooperative magnetism by limiting the inter-cluster interactions even in mixed halide/oxide compounds. However antiferromagnetic interactions at low temperatures have been observed for $LuNb_6Cl_{18}$ that exhibits the closest Nb_6–Nb_6 distance in the $RENb_6Cl_{18}$ chloride series owing to the small size of lutetium [13].

In contrast to the molecular behavior of the M_6 cluster halides, the strong interactions between the $M_6O^i_{12}O^a_6$ units in M_6 cluster oxides, lead frequently to band structures [14]. Indeed, the ultimate condensation of these units observed for NbO [15] ($Nb_{6/2}O^{i-i-i-i}_{12/4}$ according to the Schäfer notation) induces transport properties and a superconducting transition at low temperature.

The next step of our work is to replace, in the series of M_6 cluster compounds, Cl, Br and I halogens by fluorine in order to increase the interactions between Nb_6 clusters by reducing the steric hindrance of their 18 bonded ligands. Thus, fluorine could allow stabilization of new cluster compounds with new physical properties. Among cluster compounds, Nb_6F_{15} was for a long time the only example involving fluorine ligands reported in the literature [16]. In this paper, we shall present the crystal structure of two new chlorofluorides: $KNb_6Cl_{10}F_5$ and $CsNb_6Cl_8F_7$. These structural results complete those that we have recently obtained for $[Na_2NbF_6$–$(Nb_6Cl_8F_7)]$ [17] and $Nb_6Cl_{15-x}F_x$ [18]. They allow discussion of the structural influence of fluorine on the stabilization of compounds containing the M_6L_{15}-framework type in the Nb–Cl–F system, and the progressive evolution from the Ta_6Cl_{15} (Fig. 2a) structure-type [6] to

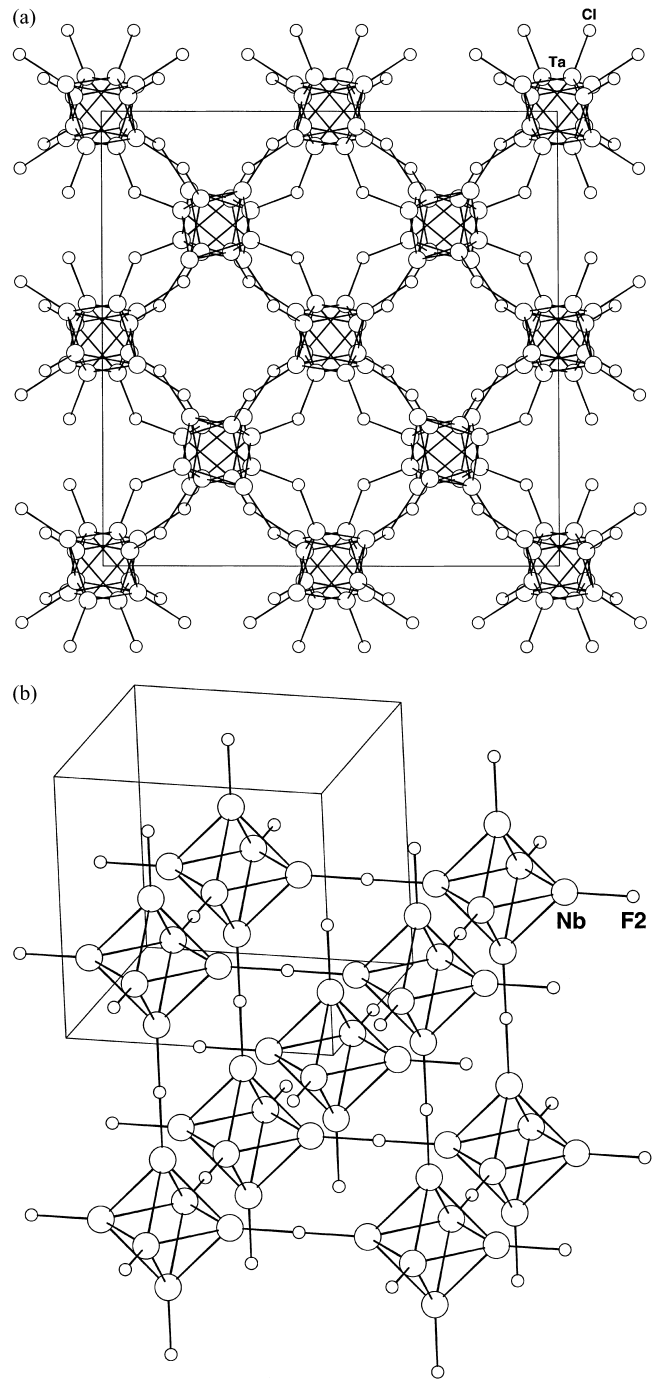

Fig. 2. (a) Projection along [0 0 1] of the Ta_6Cl_{15} structure; (b) interconnection of the units in the Nb_6F_{15} structure. For clarity, the inner ligands are not represented.

the Nb_6F_{15} (Fig. 2b) one, which differ in the kind of cluster interconnections.

2. Experimental

2.1. Synthesis

The two quaternary chlorofluorides $KNb_6Cl_{10}F_5$ and $CsNb_6Cl_8F_7$ were prepared by solid state reaction from stoichiometric mixtures of KCl or CsCl (Merck, Pro Analysi), NbF_5 (Aldrich, 98%), $NbCl_5$ (Ventron, 99.9985%), and Nb powder (Ventron, m2N8). The starting powders were handled under an inert atmosphere. After grinding, the sample was formed as a pellet, and introduced into a niobium container (Plansee) which was then welded under argon and encapsulated in an evacuated silica tube. The final product was obtained as a black microcrystalline powder after 3 days of reaction, at a temperature ranging from 700 to 800°C depending on the starting system. Energy Dispersive Spectrometry analysis performed on several selected crystals showed that they all contained the expected elements with a stoichiometry in agreement with the initial one. Additional lines in the X-ray powder diffraction pattern of $CsNb_6Cl_8F_7$ could be attributed to another orthorhombic Nb_6 cluster phase crystallizing in the Cs–Nb–Cl–F system [19]. For $KNb_6Cl_{10}F_5$, the X-ray powder diffraction pattern did not exhibit additional lines.

A similar procedure had been used to synthesize the other M_6 cluster chlorofluorides discussed in this paper [17,18].

2.2. Structure determination

The single crystals used have been synthesized according to the aforementioned procedure. The data collections have been carried out on a Nonius KappaCCD X-ray area-detector diffractometer with Mo Kα radiation ($\lambda = 0.71073$ Å). Details of the intensity measurements are reported in Table 1. Both compounds crystallize in the cubic system, with an I and P network for $KNb_6Cl_{10}F_5$ and $CsNb_6Cl_8F_7$, respectively. Once the data processing had been performed through the KappaCCD analysis software [20], the cell parameters have been refined to the following values: $a = 19.589(1)$ and $a = 8.2743(3)$ Å for $KNb_6Cl_{10}F_5$ and $CsNb_6Cl_8F_7$, respectively. An effective absorption correction has been carried out through Scalepack [21]. Among the possible space groups deduced from the extinction conditions, the refinement procedure has allowed to retain unambiguously the *Ia-3d* and *Pm-3m* groups for $KNb_6Cl_{10}F_5$ and $CsNb_6Cl_8F_7$, respectively. Both structures have been solved by direct methods (program SIR97 [22]). The least-squares refinement and Fourier syntheses have been performed with the beta version of JANA2000 [23] for $KNb_6Cl_{10}F_5$ and with the program CRYSTALS [24] for $CsNb_6Cl_8F_7$.

After several cycles without introducing fluorine, it turned out that the sites of all the chlorine atoms were not fully occupied within the e.s.d.'s. Fluorine was then introduced with the same positional and thermal parameters as chlorine, but the sum of their occupancies was restricted to the value corresponding to a fully occupied position. Afterwards, the first two restraints were progressively relaxed during the convergence, leading to final positions in agreement with reliable Nb–(Cl, F) inter-atomic distances. Moreover, in $CsNb_6Cl_8F_7$, the apical ligand is located on a 3d Wyckoff's position fully occupied by fluorine (F2 atom). Once the skeletons of both structures were refined, the K and Cs cations were located by Fourier difference syntheses. These atoms are disordered and several shared positions have been necessary to obtain a good agreement between observed and calculated structure factors. This disorder, which is probably static insofar as low temperature structural studies do not reveal a significant temperature dependence of the thermal parameters, can be explained by the random distribution of Cl and F on the ligand positions.

For the $KNb_6Cl_{10}F_5$ structure, a Gram–Charlier expansion [25] of the anisotropic displacement parameters of the Nb atom has been used up to the third-order in order to reduce the residual peak (0.72 $eÅ^{-3}$) that remains in the Fourier difference synthesis map at 0.58 Å from this atom. In addition, the F2, F3, and K2 atoms for this structure and all the Cs sites for the $CsNb_6Cl_8F_7$ structure have been refined with isotropic thermal parameters.

The final residual factors are $R = 3.38\%$ (for 417, $I > 3\sigma(I)$ observations versus 70 least-squares parameters) and $R = 2.06\%$ (for 324, $I > 3\sigma(I)$ observations versus 40 least-squares parameters) for $KNb_6Cl_{10}F_5$ and $CsNb_6Cl_8F_7$, respectively. Details on the structure refinement parameters are reported in Table 1. The final atomic parameters and selected geometrical parameters are reported in Tables 2, 3 and 4, respectively. Additional materials, anisotropic thermal parameters, observed and calculated structure factors can be obtained upon request from the authors.

3. Results

3.1. Structural description of $KNb_6Cl_{10}F_5$

The crystal structure of this compound is based on $(Nb_6L^{i}_{12})L^{a-a}_{6/2}$ (L = Cl, F) units linked to six adjacent ones by L^{a-a} connections (Fig. 3a). The fluorine and chlorine ligands are randomly distributed on the 12 inner and 6 apical positions. If we consider the units as independent spheres, the unit-cell (Fig. 3b) can be described by a *fcc* stacking of units, tetrahedral and octahedral vacancies being filled by another unit leading to $Z = 16$. An alternative description would be to consider a *ccc* unit-cell with a half cell-parameter. Each unit is locally surrounded by eight others forming a cube, but because of the only six possible Nb–L^{a-a}–Nb inter-unit connections, each unit is bonded to only six others. The potassium cations statistically occupy several positions close to the center of each face of the latter cube,

Table 1
Crystal data and details about the intensity measurements and the structure refinement parameters

Chemical formula	$K_{1.2(2)}Nb_6Cl_{9.9(4)}F_{5.1(4)}$	$Cs_{1.3(1)}Nb_6Cl_{8.03(2)}F_{6.97(2)}$
Formula mass (Da)	1052.23	1134.19
Space-group symmetry	Cubic	Cubic
Space-group symbol	*Ia-3d*	*Pm-3m*
Unit-cell length (Å)	19.589(1)	8.2743(3)
Cell volume (Å^3)	7517(1)	566.49(6)
Z	16	1
Density (Mg m^{-3})	3.72	3.32
Nature of the radiation	X-ray; K_α Molybdenum	X-ray; K_α Molybdenum
Radiation wavelength (Å)	0.71073	0.71073
Number of reflections used to determine the unit-cell	3011	2823
θ	1.00–40.25°	1.00–50.58°
Absorption coefficient (cm^{-1})	51.08	57.39
Temperature (K)	293	293
Crystal dimensions (mm)	0.14 × 0.09 × 0.07	0.09 × 0.07 × 0.05
Diffractometer	Nonius KappaCCD	Nonius KappaCCD
Monochromator	Graphite	Graphite
Method used to measure intensities	φ- and ω-scans	φ- and ω-scans
Absorption correction	Effective (Scalepack [21])	Effective (Scalepack [21])
Number of measured reflections	7293	1982
Number of measured reflections $I > 3\sigma(I)$	1176	925
Number of independent reflections	1981	662
R_{int} (%)	2.78	1.60
θ_{max}	40.20°	50.31°
h	0 → 14	0 → 10
k	0 → 18	0 → 12
l	2 → 24	1 → 17
Refinement on *F*		
R (%)	3.4	2.1
R_w (%)	5.2	1.6
S	1.08	1.02
Independent reflections $I > 3\sigma(I)$	417	324
Number of parameters	70	40
Weighting scheme	$w = 1/(\sigma^2(F) + 0.0016F^2)$	Chebychev polynomial
$(\Delta\sigma)_{max}$	0.01	0.09
$\Delta\rho_{max}$ (eÅ^{-3})	0.43	0.94
$\Delta\rho_{min}$ (eÅ^{-3})	−0.53	−1.09
Extinction correction	Becker–Coppens [28] type 1 Gaussian isotropic	Larson [29]
Extinction coefficient	0.17(5)	18(2)

Table 2
Fractional atomic coordinates and equivalent isotropic displacement parameters (Å^2) for $KNb_6Cl_{10}F_5$ ($U_{eq} = 1/3\sum_i[\sum_j(U^{ij}a_i^*a_j^*a_ia_j)]$)[b]

Atom	Wyckoff position	Site symmetry multiplicity	Refined multiplicity[a]	*x/a*	*y/b*	*z/c*	U_{eq}
Nb	96 h	1	1	0.5589(1)	0.03427(9)	0.0769(1)	0.0698(4)
Cl1	96 h	1	0.45(3)	0.4805(9)	0.110(1)	0.133(1)	0.083(5)
F1	96 h	1	0.55(3)	0.482(2)	0.098(2)	0.111(2)	0.086(8)
Cl2	96 h	1	0.83(2)	0.6648(3)	−0.0269(3)	0.0495(2)	0.094(2)
F2	96 h	1	0.17(2)	0.636(3)	−0.031(2)	0.054(2)	0.054(9)
Cl3	48 g	0.5	0.38(2)	5/8	0.0718(3)	0.1782(3)	0.130(3)
F3	48 g	0.5	0.12(2)	5/8	0.099(3)	0.151(3)	0.11(1)
K1	24 d	0.25	0.113(8)	1/2	1/4	1/8	0.165(9)
K2	96 h	1	0.08(2)	0.745(4)	0.055(4)	0.960(4)	0.20(4)

[a] Refined multiplicity = occupancy × site symmetry multiplicity.
[b] Calculated formula: $K_{1.2(2)}(Nb_6Cl1^i_{2.7(2)}F1^i_{3.3(2)}Cl2^i_{5.0(1)}F2^i_{1.0(1)})Cl^{a-a}_{4.5(2)/2}F^{a-a}_{1.5(2)/2}$; $K_{1.2(2)}(Nb_6Cl^i_{7.7(3)}F^i_{4.3(3)})Cl^{a-a}_{4.5(2)/2}F^{a-a}_{1.5(1)/2}$.

Table 3
Fractional atomic coordinates and equivalent isotropic displacement parameters (Å^2) for $CsNb_6Cl_8F_7$ ($U_{eq} = 1/3\sum_i[\sum_j(U^{ij}a_i^*a_j^*a_ia_j)]$)[b]

Atom	Wyckoff position	Site symmetry multiplicity	Refined multiplicity[a]	*x/a*	*y/b*	*z/c*	U_{eq}
Nb	6 e	0.125	0.1250	0	0	0.24448(3)	0.0190
Cl1	12 i	0.25	0.1669(5)	0	0.29341(7)	0.29341(7)	0.0319
F1	12 i	0.25	0.0827(5)	0	0.2531(4)	0.2531(4)	0.0295
F2	3 d	0.0625	0.0625	0	0	1/2	0.0520
Cs1	6 f	0.125	0.00156(9)	0.156(4)	1/2	1/2	0.042(4)
Cs2	24 m	0.5	0.00080(9)	0.468(2)	0.468(2)	0.312(4)	0.001(5)
Cs3	12 j	0.25	0.0034(5)	0.371(7)	0.371(7)	1/2	0.23(3)
Cs4	24 l	0.5	0.0010(2)	0.087(11)	1/2	0.44(1)	0.07(3)
Cs5	24 l	0.5	0.0082(3)	0.251(2)	1/2	0.412(2)	0.079(4)
Cs6	48 n	1	0.0117(5)	0.315(2)	0.435(2)	0.395(3)	0.116(6)

[a] Refined multiplicity = occupancy × site symmetry multiplicity.
[b] Calculated formula: $Cs_{1.3(1)}(Nb_6Cl^i_{8.03(2)}F^i_{3.97(2)})F^{a-a}_{6/2}$.

which correspond to the distorted tetrahedral sites of the *ccc* unit-cell. The coordination sphere of K atoms is constituted by 16 L (Cl, F) ligands (8 L1, 4 L2, 4 L3 for K1, and 7 L1, 4 L2, 5 L3 for K2). The K–(Cl, F) distances are within the range 2.77(2)–4.389(5) Å. As stressed before, the potassium site is statistically occupied, hence these distances correspond to an average between those observed locally for an empty and a full site. The final refinement leads to the following developed formula: $K_{1.2(2)}(Nb_6Cl1^i_{2.7(2)}F1^i_{3.3(2)}Cl2^i_{5.0(1)}F2^i_{1.0(1)})Cl^{a-a}_{4.5(2)/2}F^{a-a}_{1.5(2)/2}$. For sake of clarity, we shall round the occupancies to obtain $KNb_6Cl_{10}F_5$. The value of the VEC, equal to 16 within the standard deviations, is the optimum one, since all the bonding levels of the molecular orbital diagram are occupied.

3.2. Structural description of $CsNb_6Cl_8F_7$

The crystal structure of this compound is based on $(Nb_6L^i_{12})F^{a-a}_{6/2}$ units (Fig. 4a) linked to six adjacent others by F^{a-a} connections. Fluorine fully occupies apical positions, while the twelve inner positions are randomly occupied by chlorine and fluorine ligands. If we consider the units as independent spheres, the unit-cell (Fig. 4b) can be described by a simple cubic stacking of units. The cesium cations are statistically distributed on six positions around the center of the unit-cell. The coordination number of Cs varies between 7 and 10 depending on the position occupied. The Cs–(Cl, F) distances are within the range 2.23(6)–4.48(4) Å. Since cesium sites are statistically occupied, these distances correspond to an average between those observed locally for empty and full sites. The final refinement leads to the following developed formula: $Cs_{1.3(1)}(Nb_6Cl^i_{8.03(2)}F^i_{3.97(2)})F^{a-a}_{6/2}$, corresponding to a value of 16 within standard deviations for the VEC. For sake of clarity, in the following, we shall round the occupations to obtain $CsNb_6(Cl^i_8F^i_4)F^{a-a}_{6/2}$.

Table 4
Selected geometrical parameters (Å,°)

Compound	$KNb_6Cl_{10}F_5$	$CsNb_6Cl_8F_7$
Intra-unit distances		
Nb–Nb	2.830(3) 2.863(3)	2.8607(2)
M–L1^i		
Nb–Cl1^i; Nb–Cl1^i–Nb	2.40(2); 71.3(6) 2.45(2)	2.4613(7); 71.06(2)
Nb–F1^i; Nb–F1^i–Nb	2.07(4); 87(2) 2.04(4)	2.095(4); 86.1(2)
M–L2^i		
Nb–Cl2^i; Nb–Cl2^i–Nb	2.455(6); 71.3(2) 2.460(5)	
Nb–F2^i; Nb–F2^i–Nb	2.03(5); 86(2) 2.15(5)	
M–L^{a-a}		
Nb–Cl^{a-a}; Nb–Cl^{a-a}–Nb	2.481(5); 138.3(3)	
Nb–F^{a-a}; Nb–F^{a-a}–Nb	2.32(5); 174(3)	2.1143(3); 180

4. Discussion

4.1. Stabilization of M_6L_{15} compounds in the Nb–Cl–F system: matrix effect of fluorine

The M_6X_{15} binary halides with the $(M_6X^i_{12})X^{a-a}_{6/2}$ developed formula exhibit two different structure-types: Ta_6Cl_{15} in which the units are linked together by bent Ta–Cl^{a-a}–Ta bridges leading to an infinite network, and Nb_6F_{15} with linear Nb–F^{a-a}–Nb bridges in which two independent interpenetrating networks are derived from each other by a [1/2 1/2 1/2] translation of the cubic unit-cell. The first structure-type is obtained with M = Ta and X = Cl, Br, I, and the second only with M = Nb and X = F. It is noteworthy that in spite of great similarities between niobium and tantalum, the "Nb_6Cl_{15}" and "Ta_6F_{15}" compounds have never been obtained. In the following, we shall discuss the formation of compounds with $Nb_6(Cl, F)_{15}$ framework-types.

We have previously established [18] that the stabilization of compounds with the Ta_6Cl_{15} structure-type is directly

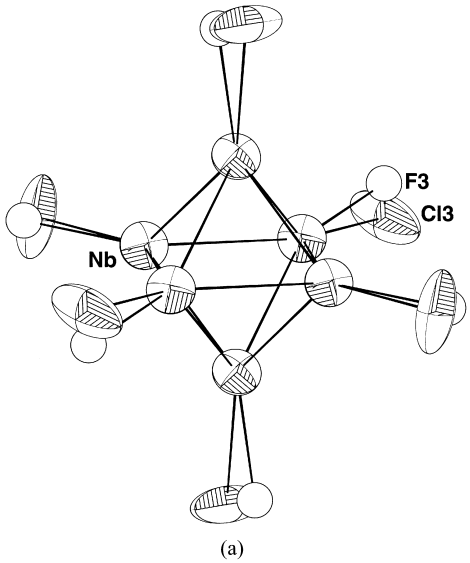

Fig. 3. (a) $(Nb_6Cl^i_8F^i_4)Cl^{a-a}_{5/2}F^{a-a}_{1/2}$ unit in $KNb_6Cl_{10}F_5$; (b) projection of the structure along the [0 0 1] direction. For clarity, the inner ligands are not represented. Only one of the two represented Cl^a or F^a positions is locally occupied. Displacement ellipsoids are shown at the 50% probability level.

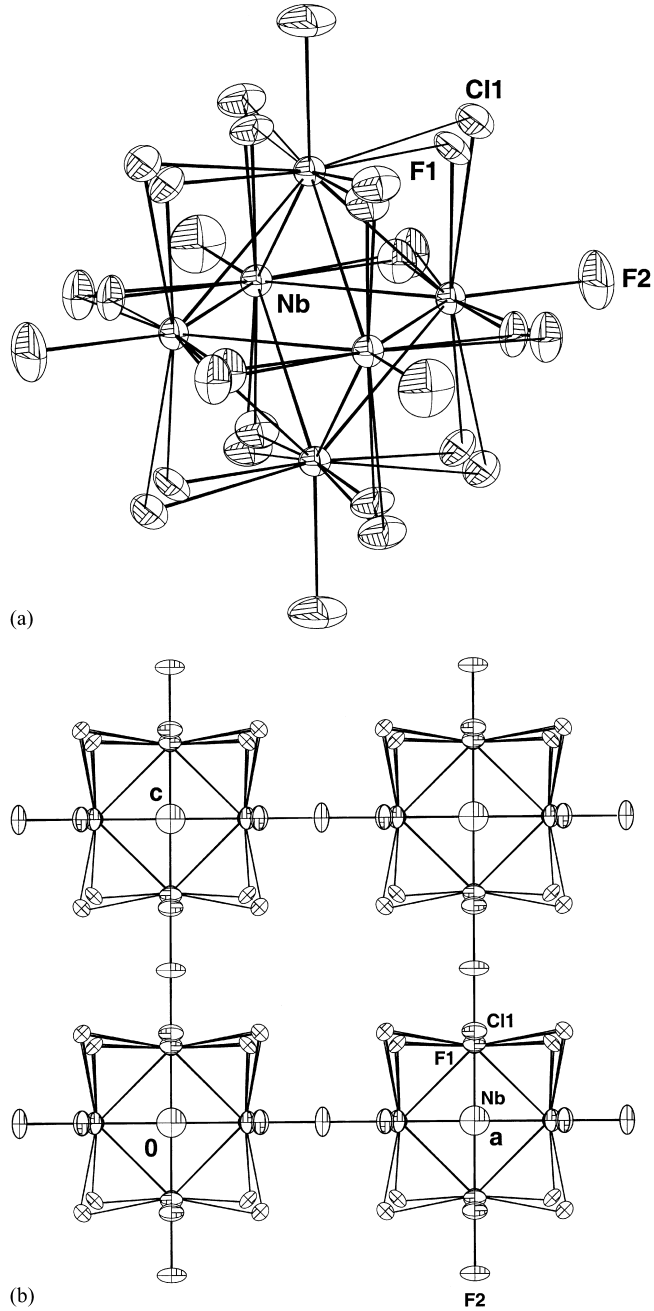

Fig. 4. (a) $(Nb_6Cl^i_8F^i_4)F^{a-a}_{6/2}$ unit in $CsNb_6Cl_8F_7$; (b) projection of the structure along the [0 0 1] direction (the cesium atoms are not represented). Only one of the two represented Cl^i or F^i positions is locally occupied. Displacement ellipsoids are shown at the 50% probability level.

related to the M–M bond lengths in the cluster, which must be sufficiently short to stabilize the $M_6Cl^i_{12}$ core. We can recall that in M_6 cluster chemistry, the M–M intra-cluster distances depend on the VEC. For instance, in chlorides containing Nb_6 clusters with a VEC equal to 16, the Nb–Nb distances are typically in the 2.91–2.93 Å range, whereas they increase to 2.95–2.96 Å for the corresponding chlorides with a VEC equal to 15 [8]. This evolution is due to a weakening of the Nb–Nb bond strengths related to the removal of one electron from the a_{2u} HOMO level exhibiting Nb–Nb bonding character. Moreover, from theoretical calculations performed on M_6L_{18} units, we have shown [12] that the Ta–Ta interactions are stronger than those for Nb–Nb, this fact being corroborated by shorter Ta–Ta bonds: for instance, they shift from 2.913 Å for $CsLuNb_6Cl_{18}$ to 2.874 Å for $CsErTa_6Cl_{18}$. Thus, in the hypothetical

"Nb_6Cl_{15}" compound with the same VEC as in Ta_6Cl_{15}, we should observe too large Nb–Nb distances for a Nb_6 cluster compound owing to the nature of the transition element. It could explain the nonexistence of such a Nb_6 chloride isostructural to Ta_6Cl_{15}. Indeed, it is not surprising that the addition of one electron into the Nb–Nb bonding states — which strengthens the Nb–Nb bond — obtained by the insertion of the small Li^+ or Na^+ cations leads to the stabilization of $LiNb_6Cl_{15}$ [26] and $NaNb_6Cl_{15}$ [27] with a Ta_6Cl_{15} framework-type.

Another relevant way to obtain a Nb_6 cluster compound isostructural to Ta_6Cl_{15} would be to replace chlorine by a smaller ligand in order to reduce the intra-cluster Nb–Nb bond lengths by a matrix effect [8]. Such a shortening can be obtained by the use of oxygen as ligand, but it implies the depopulation of the bonding molecular orbitals and then a great destabilization of the unit. The use of fluorine then becomes obvious in order to reduce the Nb–Nb bond lengths without changing the number of valence electrons in the Nb–Nb bonding states. This aim was successfully achieved through the synthesis of $Nb_6Cl_{15-x}F_x$, isotypical with Ta_6Cl_{15}, the structures of which have been determined for $x = 2.2$ and 4.4 [18]. These two compositions effectively exhibit cluster sizes similar to those found in $LiNb_6Cl_{15}$ and $NaNb_6Cl_{15}$ (see Table 5). Since we have not obtained $Nb_6Cl_{15-x}F_x$ for $x < 2.2$, we can assume that this value is the minimum one to synthesize a niobium chlorofluoride with a Ta_6Cl_{15} structure-type.

4.2. Disposition of F ligand in the M_6L_{18} unit and its influence on the inter-unit connections upon increasing the F/Cl ratio

The structures of Nb_6 chlorofluorides display two kinds of Nb_6L_{15} sub-networks based on $Nb_6(Cl^i, F^i)_{12}$ cores interconnected *via* F^{a-a} and/or Cl^{a-a} bridges. We shall compare in the following, the crystal structures of $Nb_6Cl_{15-x}F_x$ (*Ia-3d*) [18], $KNb_6Cl_{10}F_5$ (*Ia-3d*) and $CsNb_6Cl_8F_7$ (*Pm-3m*) (present work), and $[Na_2NbF_6–(Nb_6Cl_8F_7)]$ (*Pm-3m*) [17], in order to analyze the disposition of fluorine around the Nb_6 cluster upon increasing the F/Cl *ratio*. In particular, we shall show that the progressive decrease of the steric hindrance of the Nb_6L_{18} units obtained by fluorine substitution influences, also, the kind of cluster interconnections, and leads to a competition between bent bridges encountered in Ta_6Cl_{15} (*Ia-3d*) [6], and linear ones encountered in Nb_6F_{15} (*Im-3m*) [16]. We shall also explain how the increase of the F/Cl *ratio* in the apical positions strongly distorts the Ta_6Cl_{15} framework to finally give new structure-types derived from the Nb_6F_{15} one.

4.2.1. $Nb_6Cl_{15-x}F_x$ (space group Ia-3d)

In the crystal structures of $Nb_6Cl_{15-x}F_x$ (VEC = 15) determined for $x = 2.2$ and 4.4 [18], F is randomly distributed on the inner positions for both x-values, but is also randomly distributed on apical positions for $x = 4.4$. The two corresponding developed formulae are:

Table 5
Structural data on chloride, fluoride and chlorofluoride compounds containing M_6 clusters

Compound	Space group and unit-cell constants (Å)	VEC	Developed formula	M–M (Å)	Average M–M (Å)
$NaNb_6Cl_{15}$ [27]	*Ia-3d* $a = 20.417(2)$ $Z = 16$	16	$Na(Nb_6Cl^i_{12})Cl^{a-a}_{6/2}$	2.9260(7) 2.9361(6)	2.931
Ta_6Cl_{15} [6]	*Ia-3d* $a = 20.28$ $Z = 16$	15	$(Ta_6Cl^i_{12})Cl^{a-a}_{6/2}$	2.921 2.928	2.924
$Nb_6Cl_{12.8}F_{2.2}$ [18]	*Ia-3d* $a = 20.099(1)$ $Z = 16$	15	$(Nb_6Cl^i_{9.8}F^i_{2.2})Cl^{a-a}_{6/2}$	2.937(2) 2.924(2)	2.930
$Nb_6Cl_{9.6}F_{4.4}$ [18]	*Ia-3d* $a = 19.589(1)$ $Z = 16$	15	$(Nb_6Cl^i_{8.4}F^i_{3.6})Cl^{a-a}_{4.4/2}F^{a-a}_{1.6/2}$	2.930(4) 2.907(3)	2.918
$KNb_6Cl_{10}F_5$ (present work)	*Ia-3d* $a = 19.589(1)$ $Z = 16$	16	$K_{1.2}(Nb_6Cl^i_{7.7}F^i_{4.3})Cl^{a-a}_{4.5/2}F^{a-a}_{1.5/2}$	2.830(3) 2.863(3)	2.846
$CsNb_6Cl_8F_7$ (present work)	*Pm-3m* $a = 8.2742(3)$ $Z = 2$	16	$Cs_{1.3}(Nb_6Cl^i_{8.03}F^i_{3.97})F^{a-a}_{6/2}$	2.8608(2)	
$Na_2Nb_7Cl_8F_{13}$ [17]	*Pm-3m* $a = 8.2005(9)$ $Z = 1$	15 or 16	$[Na_2NbF_6–(Nb_6Cl^i_{7.9}F^i_{4.1})F^{a-a}_{6/2}]$	2.831(2)	
Nb_6F_{15} [16]	*Im-3m* $a = 8.190$ $Z = 2$	15	$(Nb_6F^i_{12})F^{a-a}_{6/2}$	2.80	

$(Nb_6Cl^i_{9.8}F^i_{2.2})Cl^{a-a}_{6/2}$ and $(Nb_6Cl^i_{8.4}F^i_{3.6})Cl^{a-a}_{4.4/2}F^{a-a}_{1.6/2}$. From these results, we can speculate that F preferentially occupies, at low content, inner positions, while at higher content of fluorine, it starts to occupy also apical positions. Unfortunately, for both $Nb_6Cl_{15-x}F_x$ structures, no actual local Nb–Cl or Nb–F distances are available for discussion insofar as F and Cl have not been structurally discriminated.

4.2.2. $KNb_6Cl_{10}F_5$ (space group Ia-3d)

$KNb_6Cl_{10}F_5$, with the developed formula $K_{1.2(2)}(Nb_6Cl^i_{7.7(3)}F^i_{4.3(3)})Cl^{a-a}_{4.5(2)/2}F^{a-a}_{1.5(1)/2}$, is characterized by a random distribution of fluorine on inner and apical positions. As the VEC per cluster (16) in this chlorofluoride is the same as in the aforementioned isostructural $NaNb_6Cl_{15}$ compound, the difference between their corresponding intra-unit distances lies only with the structural influence of fluorine, assuming that the counter-cation perturbation is negligible. The comparison between these distances allows quantification of the effect of fluorine substitution on the bond lengths and on the unit interconnections. For $KNb_6Cl_{10}F_5$, the Nb–Cl^i distances are close to those encountered in $NaNb_6Cl_{15}$ (2.451(9) Å), while the Nb–Cl^{a-a} distance is shorter than in the latter compound (2.609(1) Å). This feature is a good demonstration of the existence of L^i–L^a steric interactions around the Nb_6 cluster. Indeed, the presence of inner fluorine reduces the steric hindrance around the cluster for chlorine in apical positions, leading to shorter Nb–Cl^{a-a} bond length. We can also point out that while the Nb–Cl^{a-a}–Nb angle is equal to 138.3(3)° in $KNb_6Cl_{10}F_5$, as in $NaNb_6Cl_{15}$ (139.07°), the Nb–F^{a-a}–Nb angle is very close to 180°, like in Nb_6F_{15} or $[Na_2NbF_6–(Nb_6Cl_8F_7)]$. This experimental result must be attributed to a specificity of fluorine in Nb_6 cluster chemistry: a fluorine ligand in apical–apical position (F^{a-a}) leads to a linear Nb–F^{a-a}–Nb bridge, whatever the localization of the other adjacent interconnected units. Nevertheless, a similar discussion cannot be performed on the Nb–F intra-unit distances, since the kind of unit interconnections and the VEC value per cluster are different in $KNb_6Cl_{10}F_5$ and in Nb_6F_{15}, which prevents their comparison.

4.2.3. $CsNb_6Cl_8F_7$ (space group Pm-3m)

In this compound, fluorine is randomly distributed on inner positions and fully occupies the apical ones with Nb–F^{a-a}–Nb angles being strictly equal to 180°. The developed formula $(Cs_{1.3(1)}(Nb_6Cl^i_{8.03(2)}F^i_{3.97(2)})F^{a-a}_{6/2})$ reveals a similar F^i/Cl^i *ratio* as in $KNb_6Cl_{10}F_5$. We have previously found [13] that the Nb–L^a bond lengths influence indirectly the Nb–Nb ones by L^a/L^i repulsions: for a $Nb_6L^i_{12}$ core, the apical ligand interacts with the inner ligands influencing the Nb–Nb bond length. In $CsNb_6Cl_8F_7$ and $KNb_6Cl_{10}F_5$, the Nb–Nb and Nb–L^i inter-atomic distances are similar despite a different fluorine occupancy on apical positions. This means that the approximate value of 2 for the Cl^i/F^i ratio observed in chlorofluorides is optimum to drastically decrease the L^a/L^i steric repulsions whatever the Cl/F *ratio*

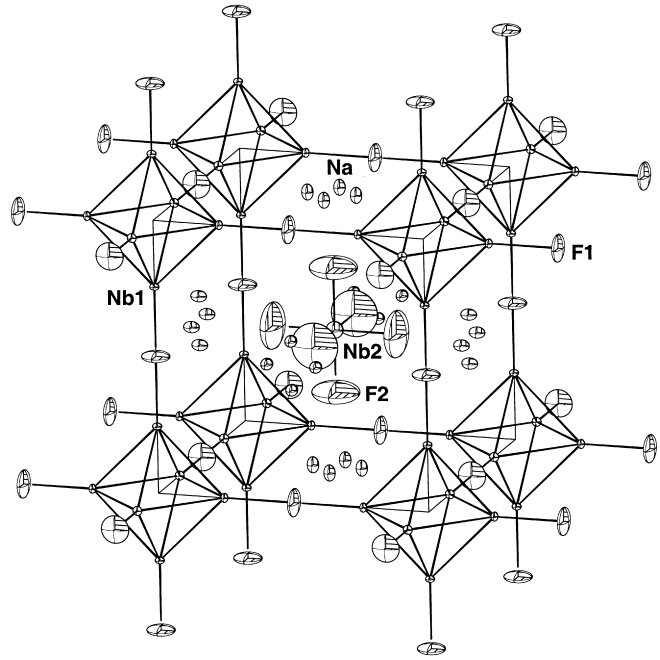

Fig. 5. Representation of the $[Na_2NbF_6–(Nb_6Cl_8F_7)]$ unit-cell [17]. For sake of clarity, the inner ligands are not represented. Displacement ellipsoids are shown at the 50% probability level.

on apical positions. The bond length Nb–F^a in $CsNb_6Cl_8F_7$ is shorter than in $KNb_6Cl_{10}F_5$. This point, which cannot be attributed to F^a/L^i interactions, may be explained by the disposition of bridges around the cluster. Indeed, in $CsNb_6Cl_8F_7$, the interconnections of the units along the four-fold axis of the cluster prevent the stretching of the Nb–F^a bond against the interconnections imposed by the Cl^a ligands along the {1 1 1} directions in $KNb_6Cl_{10}F_5$.

4.2.4. $[Na_2NbF_6–(Nb_6Cl_8F_7)]$ (space group Pm-3m)

This double salt $[Na_2NbF_6–(Nb_6Cl^i_{7.9}F^i_{4.1})F^{a-a}_{6/2}]$ (Fig. 5), which has a cluster network with NbF_6^{n-} entities and sodium cations, exhibits approximately the same Cl/F ligand arrangement as in $CsNb_6Cl_8F_7$. As a consequence, the unit stackings are the same in both compounds and their unit-cell parameters are very close.

It must be stressed that the F^i/Cl^i *ratio* is the same in all the chlorofluorides that we present here (within the standard deviation), except obviously in $Nb_6Cl_{12.8}F_{2.2}$, since its fluorine content is low. This specific *ratio* must correspond to the optimized distribution of fluorine and chlorine around the cluster to stabilize the M_6L_{18} unit.

4.3. Influence of the fluorine on the unit stacking and on the cationic sites

Under the assumption of a *ccc* network of identical spheres, the structure of chlorofluorides with a Ta_6Cl_{15} framework type can be described by a rhombohedral sub-unit-cell with $a \approx 8.5$ Å and $\alpha = 109°28'$ (Fig. 6). The

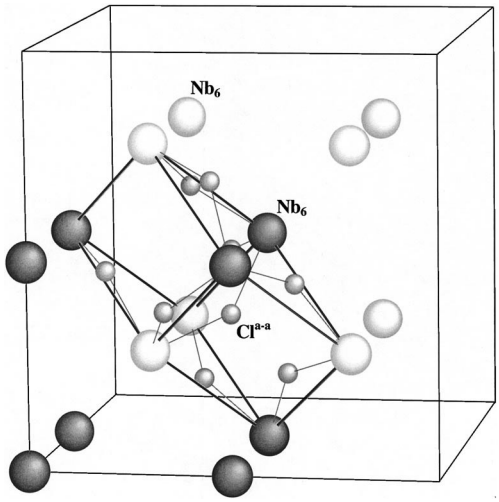

Fig. 6. Schematic representation of a rhombohedral unit-cell in $Nb_6Cl_{15-x}F_x$ considering the $Nb_6L^i_{12}$ cores as independent spheres and a *ccc* stacking.

replacement of bent Nb–$Cl^{a–a}$–Nb bridges by linear Nb–$F^{a–a}$–Nb ones implies locally structural constraints. When the fluorine ratio increases, the rhombohedral sub-unit-cell becomes more constrained leading to a spatial reorganization of the Nb–$F^{a–a}$–Nb bonds with a structural transition towards a primitive cubic framework with the same *a* parameter. From the structural results reported here, the rhombohedral sub-unit-cell subsists up to about two Nb–$F^{a–a}$–Nb bridges per unit, while the cubic one exists only when all the apical–apical positions are occupied by fluorine. Between these two limits, new structure-types are obtained like for instance the orthorhombic $Cs_xNb_6Cl_{9.8}F_{5.2}$ recently isolated [19].

In $Nb_6Cl_{15-x}F_x$ and $KNb_6Cl_{10}F_5$, the interstice located at the center of the rhombohedral sub-unit-cell described above is occupied by a $L^{a–a}$ ligand, whereas the center of the primitive cubic unit-cell is filled by large entities, like cesium cations in $CsNb_6Cl_8F_7$ or NbF_6^{n-} anionic octahedra in $[Na_2NbF_6–(Nb_6Cl_8F_7)]$. Notice that Nb_6F_{15} can be described by two $(Nb_6Cl_8F_7)$ networks derived from each other by a [1/2 1/2 1/2] translation, in which the chlorine atoms would be substituted by fluorines. Consequently, we get a body centered structure which can be viewed as the superimposition of two sub-networks isostructural to $Nb_6Cl_8F_7$.

5. Concluding remarks

From the aforementioned structural results concerning Nb_6 chlorofluorides, we can conclude that the fluorine ligand has an important steric influence on the $Nb_6(Cl, F)_{18}$ units even for low values of the F/Cl *ratio*. In addition, it turns out that for all the Nb_6 chlorofluorides, the Nb–$F^{a–a}$–Nb bridges between the units are linear. Thus, this linear inter-unit connection via fluorine seems to be a characteristic of this element in Nb_6 cluster chemistry.

The high oxidation state found for niobium in the $(NbF_6)^{n-}$ entity in $[Na_2NbF_6–(Nb_6Cl_8F_7)]$, hence for a high F/Cl ratio, could be attributed to the high electronegativity of fluorine. Indeed, in the latter compound, $(NbF_6)^{n-}$ anions (with Nb^{+4} or Nb^{+5}) coexist with Nb_6L_{18} units (with $Nb^{+2.33}$). Since these $(NbF_6)^{n-}$ entities and Nb_6L_{18} units are the basic building blocks of the usual fluoroniobates and Nb_6 halides, respectively, one can expect a new field of research at the boundary between these two chemistries. In such chlorofluorides, there could be a competition between the physical properties of the two different sub-networks. Another possibility should be, for instance, to associate in the same compound an Nb_6 cluster fluoride network with another d element sub-network usually encountered in $A_xM_yF_z$ fluorides (M = d element) in order to favor their interaction.

Acknowledgements

We would like to thank the "Centre de Diffractométrie de l'Université de Rennes 1" for the data collection on the Nonius KappaCCD X-ray diffractometer. In particular, the useful advice of Dr. T. Roisnel is gratefully acknowledged. We are also very much indebted to C. Derouet for his technical help during the synthesis of the samples and to "Fondation Langlois" for its financial support.

References

[1] D. Babel, A. Tressaud, in: P. Hagenmuller (Ed.), Material Science Series, Inorganic Solid Fluorides, Academic Press, New York, 1985, p. 77.
[2] M.B. Bournonville, D. Bizot, J. Chassaing, M. Carton, J. Solid State Chem. 62 (1986) 212.
[3] J. Chassaing, C. Monteil, D. Bizot, J. Solid State Chem. 43 (1982) 327.
[4] P.A. Pauling, J.H. Sturdivant, L. Pauling, J. Am. Chem. Soc. 72 (1950) 5477.
[5] A. Simon, H.-G.v. Schnering, H. Schäfer, Z. Anorg. Allg. Chem. 361 (1968) 235.
[6] D. Bauer, H.-G.v. Schnering, Z. Anorg. Allg. Chem. 361 (1968) 259.
[7] H. Schäfer, H.-G.v. Schnering, Angew. Chem. 76 (1964) 833.
[8] C. Perrin, S. Cordier, S. Ihmaïne, M. Sergent, J. Alloys Comp. 229 (1995) 123.
[9] S. Cordier, C. Perrin, M. Sergent, Mater. Res. Bull. 31 (1997) 25.
[10] S. Cordier, C. Perrin, M. Sergent, J. Solid State Chem. 120 (1995) 43.
[11] S. Cordier, C. Perrin, M. Sergent, Eur. J. Solid State Inorg. Chem. 31 (1994) 1049.
[12] F. Ogliaro, S. Cordier, J.-F. Halet, C. Perrin, J.-Y. Saillard, M. Sergent, Inorg. Chem. 37 (1998) 6199.
[13] S. Ihmaïne, C. Perrin, O. Peña, M. Sergent, J. Less Common Met. 137 (1988) 241.
[14] G.V. Vajenine, A. Simon, Inorg. Chem. 38 (1999) 3463.
[15] A.L. Bowman, T.C. Wallace, J.L. Yarnell, R.G. Wenzel, Acta Crystallogr. 21 (1966) 843.
[16] H. Schäfer, H.-G.v. Schnering, K.J. Niehus, H.G. Nieder-Vahrenholz, J. Less Common Met. 9 (1965) 95.

[17] S. Cordier, A. Simon, Solid State Sci. 1 (4) (1999) 199.
[18] L. Le Polles, S. Cordier, C. Perrin, M. Sergent, C.R. Acad. Sci. Paris, Ser. II c 2 (1999) 661.
[19] S. Cordier, O. Hernandez, C. Perrin, A. Simon, $Cs_xNb_6Cl_{9.8}F_{5.2}$, orthorhombic, *Pmma*, $a = 17.532(4)$ Å, $b = 12.983(3)$ Å, $c = 8.793(2)$ Å and $Z = 4$, in preparation.
[20] Nonius, COLLECT, DENZO, SCALEPACK, SORTAV: KappaCCD Program Package, Nonius B.V., Delft, The Netherlands, 1999.
[21] Z. Otwinowski, W. Minor, Processing of X-ray diffraction data collected in oscillation mode, in: C.W. Carter Jr., R.M. Sweet (Eds.), Methods in Enzymology, Macromolecular Crystallography, Part A, Vol. 276, Academic Press, New York, 1997, pp. 307–326.
[22] G. Cascarano, A. Altomare, C. Giacovazzo, A. Guagliardi, A.G.G. Moliterni, D. Siliqi, M.C. Burla, G. Polidori, M. Camalli, Acta Crystallogr. A 52 (1996) C79.
[23] V. Petříček, M. Dušek, JANA2000: Crystallographic Computing System, Institute of Physics, ASCR, Praha, Czech Republic, 2000.
[24] D.J. Watkin, C.K. Prout, J.R. Carruthers, P.W. Betteridge, CRYSTALS Issue 10, Chemical Crystallography Laboratory, University of Oxford, Oxford, 1996.
[25] K.N. Trueblood, H.-B. Bürgi, H. Burzlaff, J.D. Dunitz, C.M. Gramaccioli, H.H. Schulz, U. Shmueli, S.C. Abrahams, Acta Crystallogr. A 52 (1996) 770.
[26] B. Bajan, G. Balzer, H.-J. Meyer, Z. Anorg. Allg. Chem. 623 (1997) 1723.
[27] M.E. Sägebarth, A. Simon, H. Imoto, W. Weppner, G. Kliche, Z. Anorg. Allg. Chem. 621 (1995) 1589.
[28] P.J. Becker, P. Coppens, Acta Crystallogr. A 30 (1974) 129.
[29] A.C. Larson, in: F.R. Ahmed (Ed.), Crystallographic Computing, Munksgaard, Copenhagen, 1970, pp. 291–294.